

# Generation and propagation characteristics of a localized hollow beam

Meng Xia<sup>1</sup>, Zhizhang Wang<sup>1</sup>, Yaling Yin<sup>1</sup>, Qi Zhou<sup>2</sup>, Yong Xia<sup>1,3</sup> and Jianping Yin<sup>1</sup>

<sup>1</sup> State Key Laboratory of Precise Spectroscopy, School of Physics and Materials Science, East China Normal University, Shanghai 200062, People's Republic of China

<sup>2</sup> College of Science, East China University of Technology, Nanchang, Jiangxi 330013, People's Republic of China

<sup>3</sup> Collaborative Innovation Center of Extreme Optics, Shanxi University, Taiyuan, Shanxi 030006, People's Republic of China

E-mail: [yxia@phy.ecnu.edu.cn](mailto:yxia@phy.ecnu.edu.cn)

Accepted for publication 7 February 2018

Published 3 April 2018



CrossMark

## Abstract

A succinct experimental scheme is demonstrated to generate a localized hollow beam by using a  $\pi$ -phase binary bitmap and a convergent thin lens. The experimental results show that the aspect ratio of the dark-spot size of the hollow beam can be effectively controlled by the focal length of the lens. The measured beam profiles in free space also agree with the theoretical modeling. The studies hold great promise that such a hollow beam can be used to cool trapped atoms (or molecules) by Sisyphus cooling and to achieve an optically-trapped Bose–Einstein condensate by optical-potential evaporative cooling.

Keywords: localized hollow beam, binary bitmaps, aspect ratio, laser trapping

(Some figures may appear in colour only in the online journal)

## 1. Introduction

Dark hollow beams (DHBs) have novel and unique physical features such as a ring-shape intensity profile, a central phase singularity, spatial propagation invariance, and spin and orbital angular momentum [1]. As a result, DHBs have attracted considerable attention for a wide range of applications in areas of particle manipulation [1–6], nanolithography and nanofabrication [7], and high-resolution optical imaging [8]. Recently, hollow beams with circular (or elliptical) symmetry, and radial (or azimuthal) polarization, have been extensively studied for elliptical Laguerre–Gaussian beams [9, 10], Mathieu beams [11, 12], vector hollow beams [13–15], localized hollow beams (LHBs) [16], and so on. One particular interest concerning LHBs is how to generate them experimentally. An LHB not only has zero-central intensity, but is also surrounded by the higher light field in all directions, like a bottle, so a LHB is also called a bottle beam. Various approaches to the generation of LHBs have been proposed since the demonstration of this beam was first realized by using the destructive interference between two light beams at the focus [16]. They were generated by the use of

nonparaxial light [17–19], holograms [16, 20], binary phase plates [21–24], conical refraction [25–29], a uniaxial crystal [30], partially coherent beams [31, 32], a spatial light modulator (SLM) [33], surface plasmon polaritons [34, 35], and a photon sieve [36], to form a desirable hollow axial structure. In phase modulation methods, the diffractive optical elements, such as the  $\pi$ -phase plate, are constructed by the binary elements or the binary bitmap of the SLM.

In 2002 we theoretically proposed a scheme using a binary circular  $\pi$ -phase plate with two zones ( $0, \pi$ ) to generate LHBs [37]. In this article, based on the idea proposed, we report on the generation of LHBs by using a binary bitmap of a SLM instead of the  $\pi$ -phase plate, so that more information is extracted from the dynamic binary images. Here we employ a SLM and a focal lens as beam-shaping, to directly translate a Gaussian laser beam into a LHB. As the SLM is controlled by a computer, our scheme is efficient and controllable. The aspect ratio of the LHB dark region can be effectively re-sized by changing the focal length of the lens. From the comparison of the calculated results with the experimental data, we validate the success of the previously proposed schemes. We also analyze the relationship of the propagation characteristics of

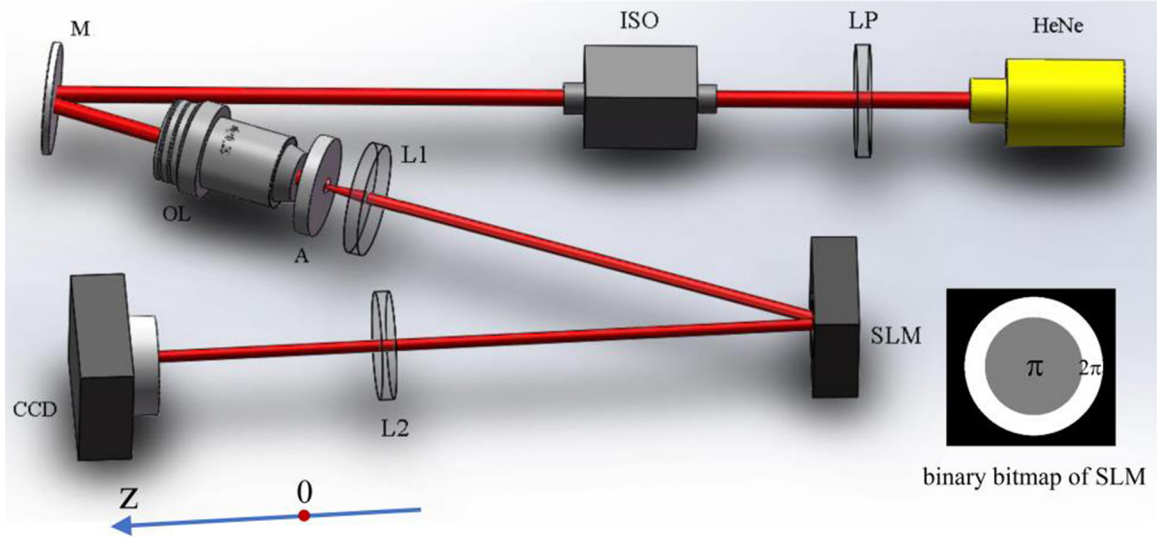


**Figure 1.** Experimental setup to produce the LHB. The abbreviations have the following meanings. HeNe: He–Ne laser; LP: linear polarizer; ISO: optical isolator; M: mirror; OL: objective lens; A: aperture;  $L_1$ ,  $L_2$ : lenses; SLM: spatial light modulator; CCD: charge-coupled device. The binary bitmap is controlled by SLM software.

the LHB generated in free space with the optical systematic parameters. The experimental and theoretical results agree well.

### 2. Experimental scheme

Figure 1 shows the experimental setup for the generation of a LHB using a SLM and a focal lens. The Gaussian laser beam (GLB) from a He–Ne laser first passes through a linear polarizer (LP) and an optical isolator. Next, it passes through a collimating and expanding beam system consisting of a spatial filter and lens  $L_1$  ( $f_1 = 400\text{mm}$ ); the spatial filter consists of microscope objectives (10 times) and an aperture ( $50\ \mu\text{m}$ ). After that, the collimated light arrives at the SLM’s screen (Model LC-R2500). The reflected light modulated by the SLM is focused by a convergent lens ( $L_2$ ). A charge-coupled device (CCD) camera is placed after lens  $L_2$  to image and record the modulated light field around the focal plane of  $L_2$ . We set the focal plane of lens  $L_2$  as the  $z = 0$  plane. The phase retardation of the SLM can be increased from 0 to  $2\pi$  by increasing the SLM’s gray level. So, based on the relation of the phase with the SLM’s gray level, we could readily encode various binary bitmaps and manipulate the incident light field.

### 3. Calculated and experimental results and discussions

Here, we briefly introduce the theory of generating the LHBs. In our scheme, the binary bitmap of the SLM acts as the  $\pi$ -phase plate with a two-zone structure ( $\pi$  and  $2\pi$ ); the  $\pi$ -phase disk and  $2\pi$ -phase ring have the same area. We adjust the outer diameter of the  $2\pi$ -phase ring to be the same size as the diameter of the incident light. Figure 1 shows that the collimated light is reflected by a phase-modulation optical element (SLM) and then converges by a lens. We assume that the

incident light is reflected by an N-portion annular phase-shifting ring shown on the SLM [38, 39]. According to diffraction theory, the normalized amplitude distribution near the focal plane of lens  $L_2$  can be defined as

$$E(\rho, u) = 2 \sum_{j=1}^N \exp(i\phi_j) \int_{r_{j-1}}^{r_j} r J_0(\rho r) g(r) \exp\left(-\frac{1}{2} i u r^2\right) dr. \tag{1}$$

Here,  $\rho$  and  $u$  are the simplified radial and axial coordinates on the imaging side, respectively,  $r$  is the radial coordinate of the objective lens’s pupil plane, and  $\phi_j$  defines the phase of zone  $j$  ( $j = 1, \dots, N$ ) on the pupil plane. The radial position of each zone is given by  $r_j$ , and  $g(r)$  is the amplitude distribution of the incident Gaussian laser beam,  $g(r) = \exp\left(-\frac{r^2}{w_0^2}\right)$ ;  $w_0$  is equal to the normalized outer radius of the phase zone,  $w_0 = 1$ . For the  $\pi$ -phase binary bitmap with two-phase zones shown in the inset of figure 1, its normalized amplitude distribution on the image side is given by [37]

$$E(\rho, u) = \frac{2}{1-e^{-1}} \int_0^1 r J_0(\rho r) \exp(-r^2) \exp\left(-\frac{1}{2} i u r^2\right) dr - \frac{4}{1-e^{-1}} \int_0^a r J_0(\rho r) \exp(-r^2) \exp\left(-\frac{1}{2} i u r^2\right) dr \tag{2}$$

where

$$\rho = \frac{2\pi}{\lambda} \left(\frac{D}{2f}\right) R \tag{3}$$

$$u = \frac{2\pi}{\lambda} \left(\frac{D}{2f}\right)^2 z \tag{4}$$

where  $D$  is the diameter of the incident Gaussian beam,  $f$  is the focal length of lens  $L_2$ , and  $a$  and 1 are the normalized radii of the  $\pi$ - and  $2\pi$ -phase zones, respectively. Then the intensity distribution of the LHB in free space can be given by

$$I = |E(\rho, u)|^2. \tag{5}$$

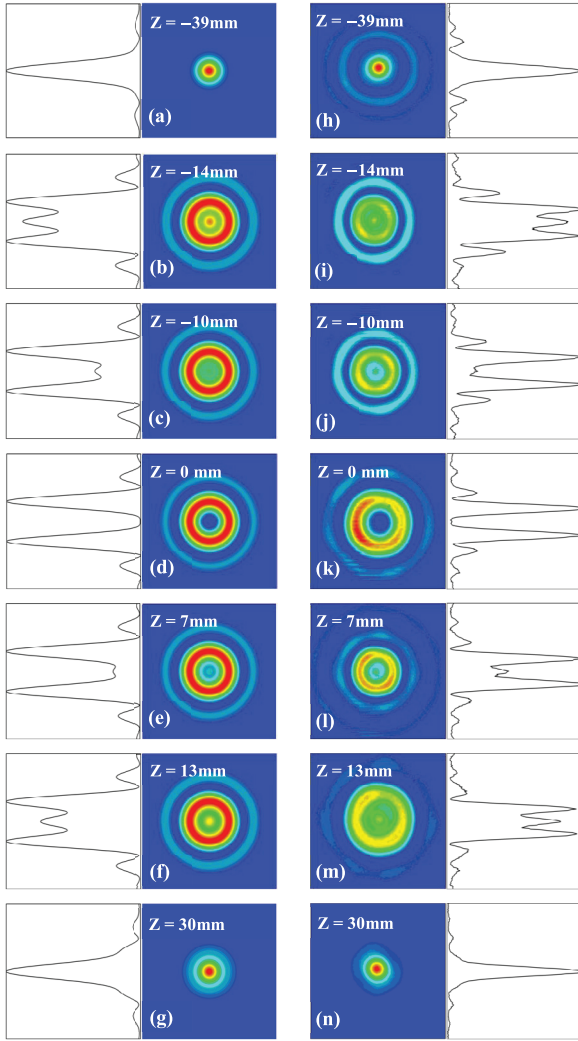


**Figure 2.** Theoretical and experimental results of 1D normalized light intensity and 2D transverse intensity distribution of the light beam's varying propagating distance  $z$  where the focal length of lens  $L_2$  is  $f = 200$  mm. Left side: (a)–(g) are the theoretical results. Right side: (h)–(n) are the experimental results.

The intensity distributions of the output light beam at a propagating distance  $z$  along the optical axis can be calculated by equations (1)–(5). The calculated one-dimensional (1D) and two-dimensional (2D) intensity distributions of the focused light beam along the propagating direction are shown in figures 2(a)–(g). From our calculations, the waist diameter of the incident GLB is  $D = 2.2$  mm (to compare with the experimental results below), the focal length of lens  $L_2$  is  $f = 200$  mm, and the wavelength of the incident GLB is  $\lambda = 632.8$  nm.

As shown in figures 2(a)–(g), the intensity distribution of the light beam in the plane of  $z = -39$  mm still displays a peak intensity in the center. But when the light beam is propagating to the position close to the focal plane of lens  $L_2$ , its center intensity gradually decreases. In the focal plane of lens  $L_2$ , the center intensity is nearly zero and a hollow beam is formed. When the propagating distance continues to move away from the focal plane, the intensity of the light beam center gradually increases. In the position  $z = 30$  mm,

the light beam is transformed to a beam that again has a peak intensity. According to figures 2(a)–(g), we can see that the incident GLB is gradually transformed into a light beam with a dark region and surrounded by the higher intensity. The light beam is nearly symmetrical around the focal plane. As a result, a LHB is formed as desired. The calculated results also show that the maximum size of the dark region appears at the focal point of the lens.

In the experiment, we set the binary bitmap of the SLM as a  $\pi$ -phase plate (as shown in figure 1) on the computer. The experimental results detected by CCD camera can be seen in figures 2(h)–(n). From figures 2(h)–(n), the light beam exhibits a Gaussian distribution. It is then gradually transformed into a beam with a dark region in the center and expanded into a Gaussian beam in the far field along the optical axis. The experimental results also show that at  $z = 0$  mm, the central intensity of the light is close to zero, and the LHB is generated around the focal length of lens  $L_2$ . It is evident that the experimental results agree well with the theoretical results (shown in figures 2(a)–(g)) within the range of allowable error. To study the propagation characteristics of the LHB in free space, we define the special parameter, the dark spot size (DSS), as the full width at half maximum (FWHM) of the radial-intensity distribution inside the notch of the LHB [1]. By analyzing the experimental data, the radius  $DSS_r$  along the radial axis of the generated LHB is about  $73.7 \mu\text{m}$  and the radius  $DSS_z$  along the axial axis is about  $26.5$  mm. The aspect ratio ( $e = DSS_z/DSS_r$ ) is  $\sim 360$ .

When the LHB is used to trap neutral particles (such as atoms and molecules) its aspect ratio can be modulated. Based on the theoretical analysis above, we know that the DSS of the generated LHB is related to the waist diameter of the incident GLB and the focal length of lens  $L_2$ . The relationships can be described as below.

$$\text{The radial radius of the DSS : } DSS_r = k_1 \frac{f}{D} (\mu\text{m}) \quad (6)$$

$$\text{The axial radius of the DSS : } DSS_z = k_2 \left( \frac{f}{D} \right)^2 (\mu\text{m}) \quad (7)$$

where  $f$  is the focal length of lens  $L_2$ ,  $D$  is the waist diameter of the incident GLB, and  $k_1$  and  $k_2$  are characteristic parameters [37].

We then verify these two relationships from the experiments, and the results are shown in figure 3. In figure 3, the solid dots are the experimental data while the linear curves are the theoretical calculated results. The focal lengths of lens  $L_2$  are chosen as  $f = 100$  mm,  $150$  mm,  $200$  mm,  $250$  mm and  $300$  mm, while fixing the waist diameter of the incident GLB at  $D = 2.2$  mm. With the focal length increasing from  $f = 100$  mm to  $f = 300$  mm at intervals of  $50$  mm,  $DSS_r$  increases from  $39 \mu\text{m}$  to  $110 \mu\text{m}$  while  $DSS_z$  increases from  $6.6$  mm to  $59.8$  mm. We find that the radial  $DSS_r$  is proportional to  $f/D$ , while the axial  $DSS_z$  is proportional to  $(f/D)^2$ . The corresponding aspect ratio of the generated LHB is changed from  $e \sim 169$  to  $e \sim 543$ . Figure 3 also shows that the longer the focal length, the larger the DSS of the generated LHB.

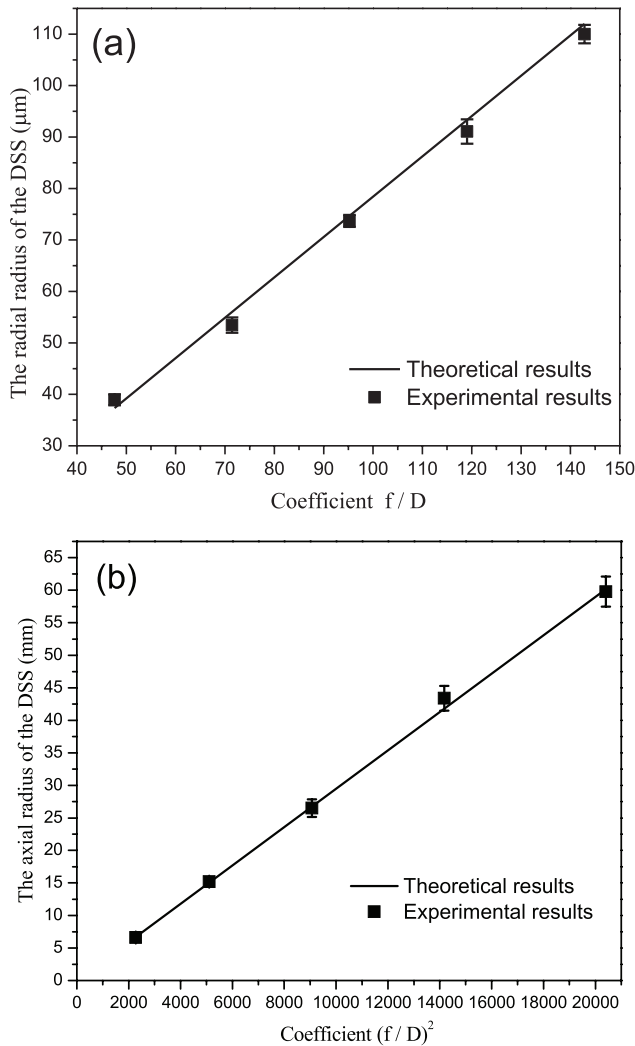


**Figure 3.** (a) The relationship of  $f/D$  with the  $DSS_r$  of the LHB in the radial direction. (b) The relationship of  $(f/D)^2$  with the  $DSS_z$  of the LHB in the axial direction. The dots are the experimental data and the lines are the theoretical results.

So, the volume of the dark region can be effectively re-sized by changing the focal length of the lens. We can also see that when the focal length  $f$  of the lens is reduced from  $f = 300$  mm to 100 mm, the radial DSS of the LHB is decreased by three times, whereas its axial DSS is reduced by nine times. In our scheme, we can obtain a LHB with a certain dark spot size ( $DSS_z$  and  $DSS_r$ ) of dozens of microns in size to meet the needs of different applications. When the above novel LHB is blue-detuned, it can be used to trap cold atoms (or molecules) from a space-compressed magneto-optical trap [40, 41]. Because the trapped volume of cold atoms (or molecules) can be compressed efficiently by reducing the focal length of the lens or increasing the power of the trapping laser beam, the LHB can be used to cool the trapped atoms by Sisyphus cooling and then to achieve an ultracold quantum gas (or even an optically-trapped Bose–Einstein condensate (BEC)) by optical-potential evaporative cooling [42]. A single neutral atom in such a blue-detuned trap can be cooled directly to about the  $\mu\text{K}$  range by intensity gradient-induced Sisyphus

cooling [43]. Also, the experimentally-formed LHB size in our scheme is very long, so this kind of long LHB has potential applications in particle manipulations, for example in the 2D trapping and 1D guiding of particles of large size [44, 45].

#### 4. Conclusions

In conclusion, we have proposed and demonstrated a succinct approach to generate a LHB by using a SLM and a focal lens. The influence of the parameters is discussed, including the waist diameter of the incident GLB and the focal length on the size of the generated LHB. We also show that the radial  $DSS_r$  is proportional to  $f/D$ , while the axial  $DSS_z$  is proportional to  $(f/D)^2$ . Compared to the phase plates, the SLM is stable and easily controlled, adjusted and integrated. Such a LHB can be used to study the interactions of the LHB with cold atoms (molecules) and BEC; it may also be used to develop optical tweezers for manipulating nanoparticles.

#### Acknowledgments

Financial support was from the Nature Science Foundation of China under 91536218 and 11374100, and the Nature Science Foundation of Shanghai Municipality under 17ZR1443000.

#### References

- [1] Yin J P, Gao W J and Zhu Y F 2003 Generation of dark hollow beams and their applications *Prog. Opt.* **45** 119–204
- [2] Padgett M J and Allen L 1999 The angular momentum of light: optical spanners and the rotational frequency shift *Opt. Quantum Electron* **31** 1–12
- [3] Khonina S N, Kotlyar V V, Skidanov R V, Soifer V A, Jefimovs K, Simonen J and Turunen J 2004 Rotation of microparticles with Bessel beams generated by diffractive elements *J. Mod. Opt.* **51** 2167–84
- [4] Shvedov V G, Hnatovsky C, Rode A V and Krolikowski W 2011 Robust trapping and manipulation of airborne particles with a bottle beam *Opt. Express* **19** 17350–56
- [5] Zhan Q 2009 Cylindrical vector beams: from mathematical concepts to applications *Adv. Opt. Photon.* **1** 1–57
- [6] Shvedov V, Davoyan A, Hnatovsky C, Engheta N and Krolikowski W 2014 A long-range polarization-controlled optical tractor beam *Nat. Photon.* **8** 846–50
- [7] Gan Z S, Cao Y Y, Evans R A and Gu M 2013 Three-dimensional deep sub-diffraction optical beam lithography with 9 nm feature size *Nat. Commun.* **4** 2061
- [8] Hell S W 2007 Far-field optical nanoscopy *Science* **316** 1153–8
- [9] Maurer C, Jesacher A, Furhapter S, Bernet S and Ritsch-Marte M 2007 Tailoring of arbitrary optical vector beams *New J. Phys.* **9** 78
- [10] Chen Y H, Liu L, Wang F, Zhao C L and Cai Y J 2014 Elliptical Laguerre–Gaussian correlated Schell model beam *Opt. Express* **22** 13975–87
- [11] Alvarez-Elizondo M B, Rodriguez-Masegosa R and Gutierrez-Vega J C 2008 Generation of Mathieu–Gauss modes with an axicon-based laser resonator *Opt. Express* **16** 18770–5
- [12] Li H R and Yin J P 2011 Generation of a vectorial Mathieu-like hollow beam with a periodically rotated polarization property *Opt. Lett.* **36** 1755–7

- [13] Ganic D, Gan X and Gu M 2003 Focusing of doughnut laser beams by a high numerical-aperture objective in a free space *Opt. Express* **11** 2747–52
- [14] Kozawa Y and Sato S 2008 Dark spot formation by vector beams *Opt. Lett.* **33** 2326–9
- [15] Khonina S N and Golub I 2012 Enlightening darkness to diffraction limit and beyond: comparison and optimization of different polarizations for dark spot generation *J. Opt. Soc. Am. A* **29** 1470–4
- [16] Arlt J and Padgett M 2000 Generation of a beam with a dark focus surrounded by regions of higher intensity: the optical bottle beam *Opt. Lett.* **25** 191–3
- [17] Bokor N and Davidson N 2007 A three-dimensional dark focal spot uniformly surrounded by light *Opt. Commun.* **279** 229–34
- [18] Wang X L, Ding J P, Qin J Q, Chen J, Fan Y X and Wang H T 2009 Configurable three-dimensional optical cage generated from cylindrical beams *Opt. Commun.* **282** 3421–5
- [19] Khonina S N and Golub I 2013 Engineering the smallest 3D symmetrical bright and dark focal spots *J. Opt. Soc. Am. A* **30** 2029–33
- [20] Zhang P, Zhang Z, Prakash J, Huang S, Hernandez D, Salazar M, Christodoulides D N and Chen Z G 2001 Trapping and transporting aerosols with a single optical bottle beam generated by moiré techniques *Opt. Lett.* **36** 1491–3
- [21] Pavelyev V, Osipov V, Kachalov D, Khonina S, Cheng W, Gaidukeviciute A and Chichkov B 2012 Diffractive optical elements for the formation of ‘light bottle’ intensity distributions *Appl. Opt.* **51** 4215–8
- [22] Ye H, Wan C, Huang K, Han T, Teng J, Ping Y S and Qiu C 2014 Creation of vectorial bottle-hollow beam using radially or azimuthally polarized light *Opt. Lett.* **39** 630–3
- [23] Hasnaoui A, Haddadi S, Fromager M, Louhibi D, Harfouche A, Cagniot E and Ait-Ameur K 2015 Transformation of a LG<sub>10</sub> beam into an optical bottle beam, *Laser Phys.* **25** 085004
- [24] Chen G et al 2016 Generation of a sub-diffraction hollow ring by shaping an azimuthally polarized wave *Sci. Rep.* **6** 37776
- [25] Cacciapuoti L, de Angelis M, Pierattini G and Tino G M 2001 Single-beam optical bottle for cold atoms using a conical lens *Eur. Phys. J. D* **14** 373–6
- [26] Kulin S, Aubin S, Christe S, Peker B, Rolston S L and Orozco L A 2001 A single hollow-beam optical trap for cold atoms *J. Opt. B* **3** 353–57
- [27] Philip G M and Viswanathan N K 2010 Generation of tunable chain of three-dimensional optical bottle beams via focused multi-ring hollow Gaussian beam *J. Opt. Soc. Am. A* **27** 2394–401
- [28] McGloin D, Spalding G C, Melville H, Sibbett W and Dholakia K 2003 Three-dimensional arrays of optical bottle beams *Opt. Commun.* **225** 215–22
- [29] Loiko Yu V, Turpin A, Kalkandjiev T K, Rafailov E U and Mompart J 2013 Generating a three-dimensional dark focus from a single conically refracted light beam *Opt. Lett.* **38** 4648–51
- [30] Shvedov V G, Hnatovsky C, Shostka N and Krolikowski W 2013 Generation of vector bottle beams with a uniaxial crystal *J. Opt. Soc. Am.* **30** 1–6
- [31] Pu J X, Liu X Y and Nemoto S 2005 Partially coherent bottle beams *Opt. Commun.* **252** 7–11
- [32] Shvedov V G, Izdebskaya Y V, Rode A V, Desyatnikov A S, Krolikowski W and Kivshar Y S 2008 Generation of optical bottle beams by incoherent white-light vortices *Opt. Express* **16** 20902–7
- [33] McGloin D, Spalding G C, Melville H, Sibbett W and Dholakia K 2003 Applications of spatial light modulators in atom optics *Opt. Express* **11** 158–66
- [34] Genevet P, Dellinger J, Blanchard R, She A, Petit M, Cluzel B, Kats M A, de Fornel F and Capasso F 2013 Generation of two-dimensional plasmonic bottle beams *Opt. Express* **21** 10295–300
- [35] Epstein I and Arie A 2014 Dynamic generation of plasmonic bottle-beams with controlled shape *Opt. Lett.* **39** 3165–8
- [36] Cheng Y G, Tong J M, Zhu J P, Liu J B, Hua S and He Y 2016 Clad photon sieve for generating localized hollow beams *Opt. Laser Eng.* **77** 18–25
- [37] Yin J P, Gao W J, Wang H F, Long Q and Wang Y Z 2002 Generations of dark hollow beams and their applications in laser cooling of atoms and all optical-type Bose–Einstein condensation *Chin. Phys.* **11** 1157–69
- [38] Sales T R M and Michael Morris G 1997 Fundamental limits of optical super resolution *Opt. Lett.* **22** 582–4
- [39] Wang H F and Gan F X 2001 High focal depth with a pure-phase apodizer *Appl. Opt.* **40** 5658–62
- [40] Raab E L, Prentiss M, Cable A, Chu S and Pritchard D E 1987 Trapping of neutral sodium atoms with radiation pressure *Phys. Rev. Lett.* **59** 2631–4
- [41] Barry J F, McCarron D J, Norrgard E B, Steinecker M H and DeMille D 2014 Magneto-optical trapping of a diatomic molecule *Nature* **512** 286–9
- [42] Yin J P 2006 Realization and research of optically-trapped quantum degenerate gases *Phys. Rep.* **430** 1–116
- [43] Yin Y L, Xia Y, Ren R M, Du X L and Yin J P 2015 Intensity-gradient induced Sisyphus cooling of a single atom in a localized hollow-beam trap *J. Phys. B* **48** 195001
- [44] Shvedov V G, Rode A V, Izdebskaya Y V, Desyatnikov A S, Krolikowski W and Kivshar Y S 2010 Giant optical manipulation *Phys. Rev. Lett.* **105** 118103
- [45] Shvedov V G, Desyatnikov A S, Rode A V, Krolikowski W and Kivshar Y S 2009 Optical guiding of absorbing nano-clusters in air *Opt. Express* **17** 5743–57